Research Article

iMedPub Journals
www.imedpub.com

Insights in Analytical Electrochemistry
ISSN 2470-9867

2018
Vol.4 No.1:7

DOI: 10.21767/2470-9867.100028

Corrosion Monitoring by Electrochemical Impedance Spectroscopy Test of Low-Cr Alloy Steel T_{22} and High-Ni Alloy HR_{224} in Nitrate Molten Salt

Angel G Fernandez* **and Abdiel Mallco**

Energy Development Center, University of Antofagasta, Av. Universidad de Antofagasta 02800, Antofagasta, Chile

***Corresponding author:** Angel G Fernandez, Energy Development Center, University of Antofagasta, Av. Universidad de Antofagasta 02800, Antofagasta, Chile, Tel: 585-395-5586; E-mail: angel.fernandez@uantof.cl

Rec date: March 29, 2018; **Acc date:** April 06, 2018; **Pub date:** April 15, 2018

Citation: Fernandez AG, Mallco A (2018) Corrosion Monitoring by Electrochemical Impedance Spectroscopy Test of Low-Cr Alloy Steel T_{22} and High-Ni Alloy HR_{224} in Nitrate Molten Salt. Insights Anal Electrochem Vol.4 No.1:7

Abstract

High temperature corrosion is one of the most important issues for materials selection, structure design and service life prediction of engineering parts that are exposed to high-temperature environments. The prevention of high temperature corrosive attacks on materials play a critical role in aspects such as reliability, quality, safety and profitability of any industrial sector associated with high temperature process and in the study case, solar energy storage market, using inorganic molten salts.

This paper proposes a corrosion monitoring technique based on Electrochemical Impedance Spectroscopy (EIS) and propose the corrosion mechanism that occurs during the test. Tests were carried out in conventional solar salt (60% $NaNO_3$+40% KNO_3) at 390°C in contact with a low Cr alloy steel (T_{22}) and in a Ni base alloy (HR_{224}). The corrosion monitoring technique performed *in situ* in contact with the salts showed a lower corrosion rate (0.0065 mm/year) in the Ni alloy compared with the low Cr alloy T_{22} (0.022 mm/year). Regarding the corrosion mechanism both steel formed a protective layer in the steel surface at the beginning of the corrosion test.

Keywords: Molten salt; Corrosion; Electrochemical impedance spectroscopy (EIS)

Introduction

The solar conditions in northern Chile, Direct Normal Irradiation (DNI) and Global Horizontal Irradiation (GHI) are the best in the world [1] **(Figure 1)**; consequently, the implementation of technologies to generate electricity based on solar sources is of particular importance. These features are very important because these salts are used in current solar technologies for storage energy and provide significant benefits because this type of storage considerably increases the performance of solar plants and provides energy at night [2].

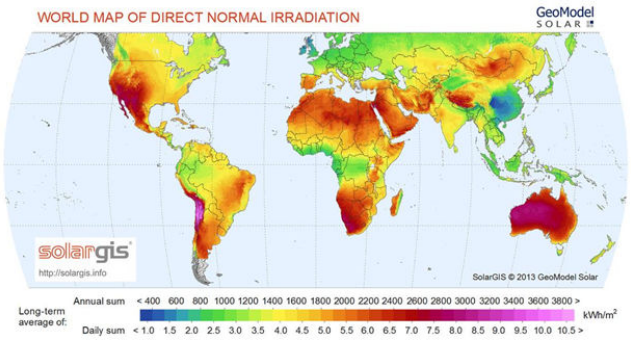

Figure 1 Map of the direct normal irradiation in the world [3].

In this context, molten salts have been selected as Thermal Energy Storage (TES) material in concentrated solar power (CSP). Molten salts are commercial mixtures operates at temperatures between 390-550°C, depending on the CSP plant selected (parabolic trough or central tower). In order to reduce the storage cost, the proposal of new container materials is needed along with the use of high resistance alloys in order to reduce the corrosion rate in CSP plant components. One of the obstacles for a successful development is the selection and reliable prediction of materials performance at the long term. In this direction the use of a corrosion monitoring technique based on electrochemical impedance spectroscopy tests have been tested in this work.

It is known that EIS is a powerful technique that has been used to determine corrosion mechanisms in aqueous corrosion of alloys and metals for decades. The method has gained popularity since it can be performed *in-situ*, and because it usually does not require any artificial acceleration of the corrosion process [4]. The greatest advantage of this technique is the low intensity of excitation signal used which causes minimal disruption in the electrochemical system state, constituting a non-destructive technique and reducing the

error associated with the measurement process. Impedance spectra obtained by this method are adjusted to an electrical circuit of a combination of resistors and capacitors (equivalent circuits) [5], in order to interpret the corrosion mechanisms.

Potentiodynamic polarization (PP) has been used to measure molten salt corrosion of stainless steels or alloys since it generates data quickly and is sensitive to very low corrosion rates [6]. The open-circuit potential (OCP) is the stable electric potential obtained between the metal surface and the electrolyte (molten salt). To initiate the PP, the metal/electrolyte system is first cathodically polarized (negative over potential from the OCP), followed by a sweep in applied potential toward anodic polarization (positive over potential from OCP). The polarization curves (applied potential vs measured current density) are then used to find the cathodic and anodic Tafel slopes [7].

The intersection of the Tafel slopes provides the corrosion potential (E_{corr}) and corrosion current density (j_{corr}), which is use to obtain the corrosion current (i_{corr}) divided by the exposed area (A).

The corrosion rate (CR) in millimeters per year can be calculated using the Stern-Geary equation (Equation 1) through Faraday's law [8-11].

$$CR = \frac{j_{corr} KEW}{\rho} \qquad Eq(1)$$

Where K is a constant equal to 3272 [mm / (A cm year)], EW is the equivalent weight of the alloy [g/mole-e-], and ρ is the alloy density [g/cm^3].

The equivalent weight of the alloy is calculated using its composition and the following equations (Equations 2 and 3).

$$EW = NEQ^{-1} \qquad Eq(2)$$

$$NEQ = \sum \left(\frac{f_i n_i}{MW_i} \right) \qquad Eq(3)$$

Where NEQ is the number of equivalent; f_i is the weight fraction; n_i is the number of electrons being transferred and MW_i is the atomic weight [12-14].

In this direction, this paper proposes a corrosion study based on Electrochemical Impedance Spectroscopy applied to a low Cr steel (T_{22}) and Ni alloy (HR_{224}) exposed to Solar Salt (60% $NaNO_3$/40% KNO_3) at thermal energy storage temperature of linear CSP plants (390°C) [15-17].

Experimental Procedure

Preparation of solar salt

The mixture of $NaNO_3$ (SQM, 99.6% refined) and KNO_3 (SQM, 99.8% refined) was prepared using 60 and 40 percent in weight respectively.

The salt mixture was immersed in a muffle furnace at 150, 250 and 350°C for 8 hours in each case, increasing the temperature by stages in order to remove the water content in the salt. Subsequently the corrosion test was carried out in alumina crucibles immersing the alloy steel (T_{22}) and HR_{224} alloy in the solar salt at 390°C during 96 hours. Detailed composition of alloys is shown in **Table 1**.

Table 1 Chemical composition of alloys T_{22} and HR_{224}.

Alloys	%wt.															
	Si	Mn	Cr	P	Mo	C	S	Ni	Fe	Co	W	Nb	Al	Ti	B	Zr
T_{22}	<0.5	0.3 - 0.6	1.9 - 2.6	0.03	0.87 - 1.13	<0.15	0.3	-	Balance	-	-	-	-	-	-	-
HR_{224}	0.3	0.5	20	-	<0.5	0.05	-	Balance	27.5	< 2	<0.5	<0.15	3.8	0.3	<0.004	0.025

Experimental set-up

A scheme of the experimental set-up for potentiostat scans is shown in **Figure 2**. Working (WE) and reference/counter (RE-CE) electrodes were immersed in the molten salt (electrolyte) and the Open Circuit Potential (OCP) was measured using a potentiostat (AUTOLAB-PGSTAT 302 N) connected to the system through a Ni-Cr wire. The values of the parameters for the electrochemical impedance test were obtained in a frequency range between 100 KHz and 5 mHz.

Figure 2 Corrosion tests by Electrochemical Impedance Spectroscopy.

Results and Discussion

The data obtained were adjusted to different models of equivalent circuits for nitrate molten salts shown in the **Figures 3 and 4**. In this case, the fit curve is matching to a protective scale on the steel surface. In this case, the transportation of ions in the scale, not the diffusion of oxidants in the electrolyte should be rate limiting. If the scale is considered as a capacitor, it is related with the double-layer capacitance at the scale/salt interface and it is represented by the equivalent circuit of **Figure 3**, where, C_{ox} represents the oxide capacitance and R_{ox}, the transfer resistance of ions in the scale.

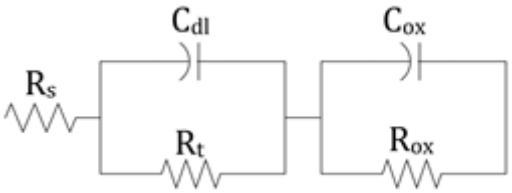

Figure 3 Equivalent circuits representing the corrosion of metals forming a protective scale in molten salts.

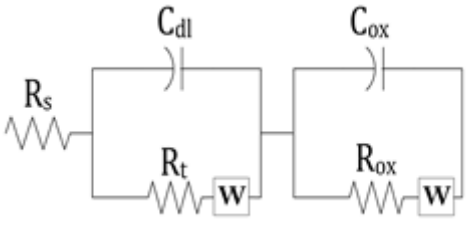

Figure 4 Equivalent circuits representing the corrossion of metals forming a protective scale with a process in both circuits in molten salts.

The electrochemical impedance for this equivalent circuit is expressed by Equation 4.

$$Z = R_S + \frac{1}{jwC_{dl} + wC_{dl}\cot(n_{dl}\frac{\pi}{2}) + \frac{1}{R_t}} + \frac{1}{jwC_{ox} + wC_{ox}\cot(\frac{\beta\pi}{2}) + \frac{1}{R_{ox}}} \quad Eq(4)$$

An usual behaviour found in molten salt corrosion is the diffusion control during the corrosion process **(Figure 4).** The diffusion of oxidants to the scale/salt interface is not fast enough to meet their consumption in the reaction. In this case, the anodic and cathodic charge transfers are a little faster process, and are not rate limiting.

The cathodic process mainly including the cathodic charge transfer and in this case Z_w (Warburg resistance) is considering and the electrochemical impedance Z can be expressed by Equation 5.

$$Z = R_S + \frac{1}{jwC_{dl} + wC_{dl}\cot(n_{dl}\frac{\pi}{2}) + \frac{1}{R_t + Z_W}} + \frac{1}{jwC_{ox} + wC_{ox}\cot(\frac{\beta\pi}{2}) + \frac{1}{R_{ox} + Z_W}} \quad Eq(5)$$

The Warburg resistance Z_w may be expressed by Equation 6.

$$Z_w = A_w(jw)^{N_w} \quad Eq(6)$$

Where A_w is the modulus of Warburg resistance associated with the solubility and diffusion coefficient of oxidants in the melt and N_w is the Warburg coefficient ($-0.5 \leq N_w < 0$). The parameter N_w is related to the diffusion direction of oxidants. When N_w is equal to -0.5 the diffusion direction of oxidants is parallel to the concentration gradient of oxidants. When $N_w > -0.5$ the diffusion direction of oxidants deviates from the concentration gradient of oxidants i.e., “tangential diffusion”.

EIS results are usually represented by Nyquist plots. The Nyquist plot represents the real part of the impedance on the abscissa and the imaginary part thereof on the ordinate axis, both at different frequencies. This method allows obtaining the electrochemical parameters through a non-destructive test and propose a corrosion mechanism for the steels tested.

Figures 5 and 6 show electrochemical impedance spectrum of the alloy Steel T_{22} and alloy HR_{224}.

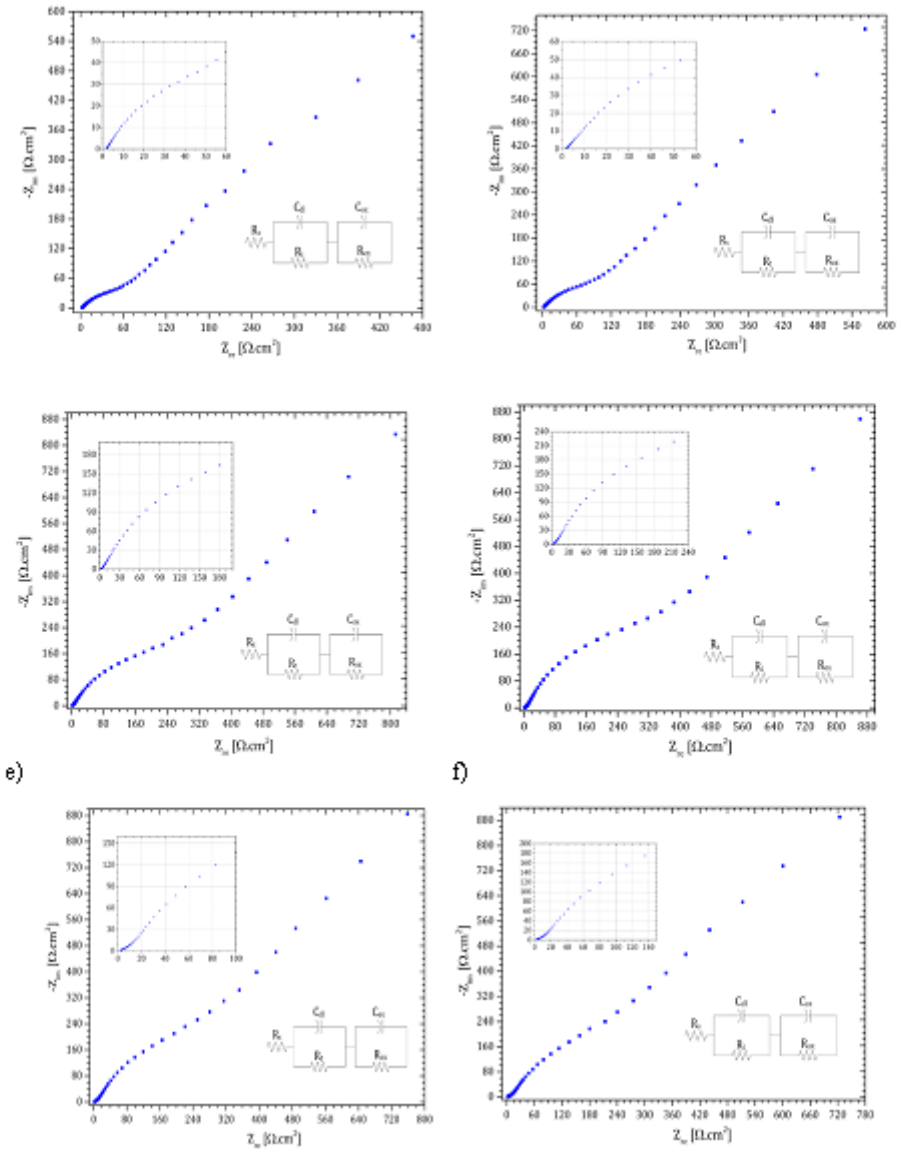

Figure 5 Equivalent Circuit of alloy steel T_{22} forming a protective layer in solar salt. a) 0 h b) 4 h c) 24 h d) 48 h e) 72 h f) 96 h.

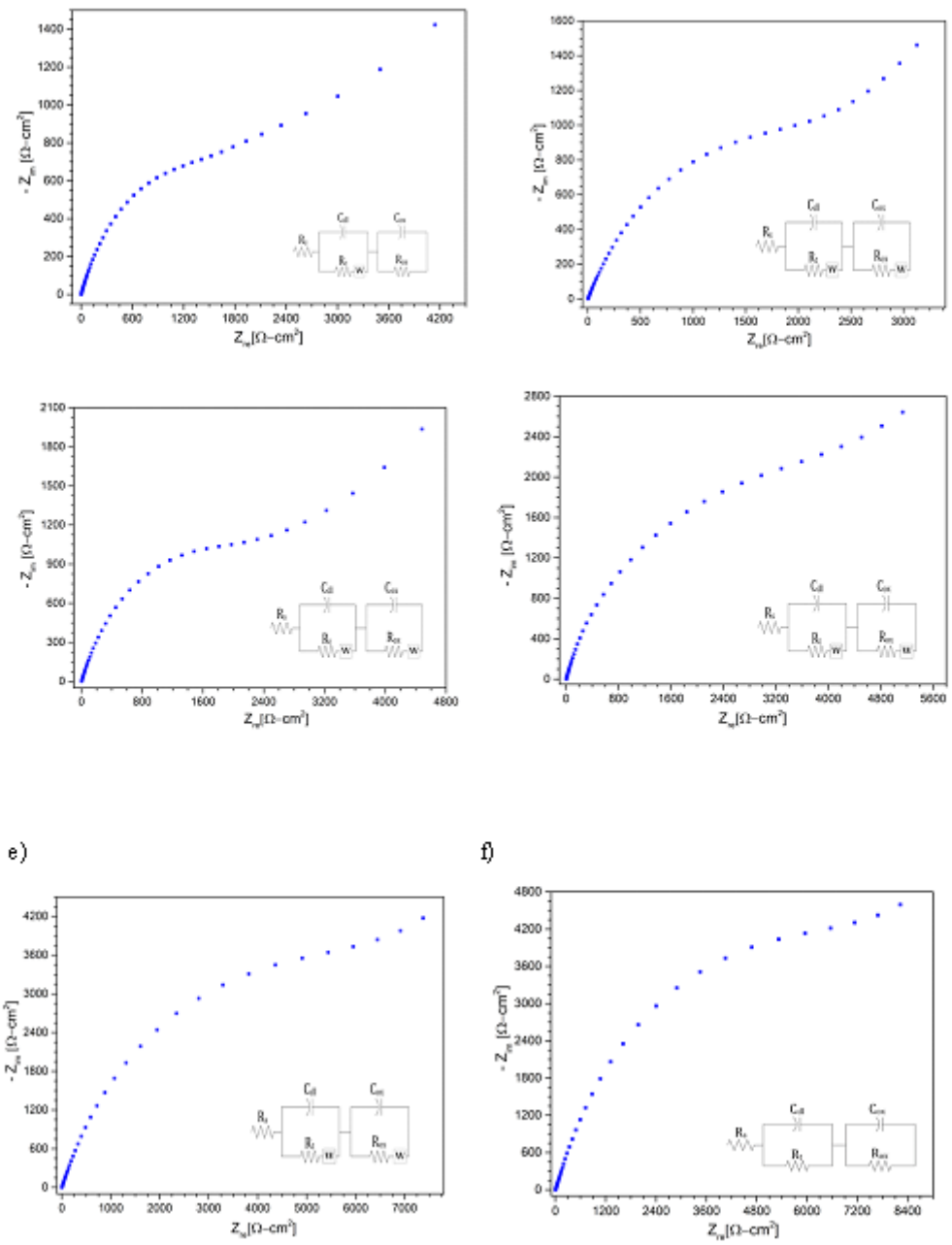

Figure 6 Equivalent Circuit of alloy steel HR_{224} forming a protective layer in solar salt. a) 0 h b) 2 h c) 4 h d) 6 h e) 24 h f) 48 h g) 72 h h) 96 h.

The electrochemical parameters in **Equation 4** were obtained by fitting the EIS based on the equivalent circuit of **Figure 3** and are listed in **Tables 2 and 3** respectively.

Table 2 Fitting results of the impedance spectra of alloy T_{22} during corrosion in the presence of $NaNO_3$ and KNO_3 at 390°C.

Time(h)	Rs(Ω-cm^2)	Rt(Ω-cm^2) × 10^3	Cdl (Ω^{-1}sndl^{-1}) x 10^{-2}	ndl	Rox(Ω-cm^2) x 10^2	Cox (Ω^{-1}snox^{-1}) x 10^{-3}	n_{ox}
0	1.82	88.1	1.4	0.61	39.2	6.1	0.72
4	1.94	87.7	1.3	0.68	10.2	5.3	0.64

24	1.89	99.9	0.068	0.98	26.2	7.1	0.56
48	1.97	93.1	0.76	0.55	15.8	11	1
72	2.08	12.4	2.7	1	8.8	7.9	0.55
96	2.07	3.7	7.6	0.65	4.4	2	0.72

Table 3 Fitting results of the impedance spectra of alloy HR_{224} during corrosion in the presence of $NaNO_3$ and KNO_3 at 390°C.

Time(h)	R_s(Ω-cm^2)	R_t(Ω-cm^2) x 10^3	C_{dl} (Ω^{-1}sndl^{-1}) x 10^{-2}	n_{dl}	W_t(Ω $s^{-1/2}$)	R_{ox}(Ω-cm^2) x 10^2	C_{ox} (Ω^{-1} snox^{-1}) x 10^{-3}	n_{ox}	W_{ox}(Ω $s^{-1/2}$)
0	1.81	4.05	4.67	0.65	626.8	1.57	0.66	0.65	-
4	2.12	2.11	0.68	0.66	-	6.48	0.37	0.83	222.1
24	1.99	2.12	0.628	0.73	-	7.17	3.59	0.61	1075
48	1.94	3.65	0.79	0.69	-	3.48	1.11	1	148.8
72	2.01	6.32	0.69	0.79	-	8.98	2.51	0.62	272.54
96	2.08	6.91	0.73	0.81	-	12.4	2.95	0.59	-

The anodic and cathodic Tafel lines required to calculate i_{corr} were obtained by using OCP followed by Linear Sweep Voltammetry (LSV) **(Table 4)**. The Tafel lines, within an interval of 120 mV with respect to the corrosion potential (E_{corr}) as well as their slopes in (mV/dec) were obtained. These LSV tests are shown in **Figure 7**.

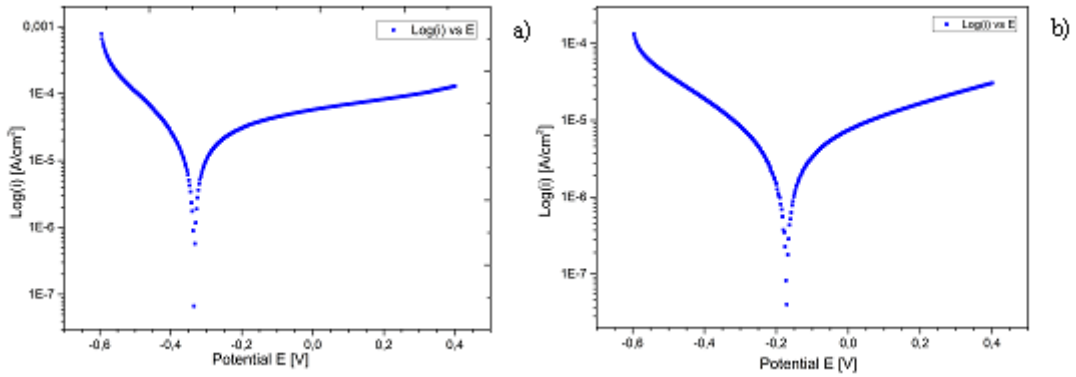

Figure 7 Polarization curves of alloys in 60 wt% $NaNO_3$ and 40 wt% KNO_3 at 390°C a) T_{22} b) HR_{224}.

Table 4 summarize the corrosive potential (Open-circuit potential (OCP), corrosion potential (E_{corr}) and corrosion current density (j_{corr}) in the steels tested and determine the corrosion rates obtained at the end of the test (96 hours).

Table 4 Corrosion data of tested alloys in 60 wt% $NaNO_3$ and 40 wt% KNO_3 at 390°C.

Alloy	O_{CP} (mV)	E_{corr} (mV)	j_{corr} (µA/cm^2)	CR (µm/year)
T_{22}	-31.84	-328.26	2.88	22.745
HR_{224}	-33.96	-171.6	0.69	6.48

Both steel tested present a low corrosion rate in the nitrate molten salt tested with 22.75 and 6.48 µm/year for T_{22} and HR_{224} respectively.

Conclusion

The results obtained by electrochemical impedance spectroscopy show the formation of a protective layer in the alloy steel T_{22} and alloy HR_{224} immersed in solar salt at 390°C during 96 hours. The spectrum was evaluated every 4 hours on the first day and every 24 hours to complete 96 hours of immersion.

The result figures have been fitted to a protective layer model. Therefore it is necessary for a better evaluation of the equivalent circuit to obtain information regarding the corrosion layer thickness produced.

A linear sweep polarization test has been performed in order to obtain the corrosion rate of the steel tested at 96 hours of immersion. It is important to point out that this test was developed *In situ* with the steel immersed in the corrosive environment so it is avoiding the steel handling and the conventional problems related with the gravimetric techniques for corrosion elucidation.

Both steel presented a low corrosion rate and it could be proposed as container material in CSP plants. On the other hand this work presents a successful development of a corrosion monitoring technique focus on Thermal Energy Storage (TES) materials at high temperature and based on Electrochemical Impedance Spectroscopy (EIS) for control storage systems.

Acknowledgment

The authors would like to acknowledge the financial support provided by CONICYT/ FONDAP 15110019 “Solar Energy Research Center” SERC-Chile and FIC-R 30413089 funded by Antofagasta Government.

References

1. Fernandez AG, Galleguillos H, Perez FJ (2014) Thermal influence in corrosion properties of Chilean solar nitrates. Sol Energy 109: 125-134.
2. Denholm P, Mehos M (2011) Enabling Greater Penetration of Solar Power via the Use of CSP with Thermal Energy Storage. United States.
3. Solargis (2018) Solar resource maps. Available from: https://solargis.com/maps-and-gis-data/download/world (accessed 28.03.2018).
4. Macdonald DD (2005) Reflections on the history of electrochemical impedance spectroscopy. Electrochimica Acta 51: 1376-1388.
5. Zeng CL, Wang W, Wu WT (2001) Electrochemical impedance models for molten salt corrosion. Corrosion Science 43: 787-801.
6. Calderon JP, Mazon OS, Bravo VMS, Gonzalez CDA, Hernandez JJR, et al. (2012) Electrochemical Performance of $Ni_{20}Cr$ Coatings Applied by Combustion Powder Spray in $ZnCl_2$-KCl Molten Salts. Int J Electrochem Sci 7: 1134-1148.
7. Zeng CL, Li J (2005) Electrochemical impedance studies of molten (0.9 Na, 0.1 k_2SO_4)-induced hot corrosion of the Ni-based superalloy M38G at 900°C in air. Electrochimica Acta 50: 5533-5538.
8. Coyle RT, Thomas TM, Lai GY (1986) Exploratory corrosion tests on alloys in molten salts at 900°C. J Mater Energy Syst 7: 345-352.
9. Solargis (2018) Solar resource maps. Available from: https://solargis.com/maps-and-gis-data/download/world (accessed 31.07.2015).
10. Gamry Instruments (2011) Getting Started with Electrochemical Corrosion Measurements. Application note, Warminster PA 18974, USA.
11. Abengoa Solar Inc (2010) Advanced Thermal Storage for Central Receivers with Supercritical Coolants. DOE Contract Report under Grant DE-FG36-08GO18149.
12. Yang Z, Garimella SV (2010) Thermal analysis of solar thermal energy storage in a molten-salt thermocline. Sol Energy 84: 974-985.
13. Padilla RV, Too YCST, Benito R, Stein W (2015) Exergetic analysis of supercritical CO_2 Brayton cycles integrated with solar central receivers. Appl Energy 148: 348-365.
14. Stekli J, Irwin L, Pitchumani R (2013) Technical challenges and opportunities for concentrating power with thermal energy storage. J Therm Sci Eng Appl 5: 021011.
15. Kruizenga A, Gill D (2014) Corrosion of iron stainless steels in molten nitrate salt. Energy Procedia 49: 878-887.
16. Neises T, Turchi C (2014) A comparison of supercritical carbon dioxide power cycle configurations with an emphasis on CSP applications. Energy Procedia 49: 1187-1196.
17. Zeng CL, Li J (2005) Electrochemical impedance studies of molten (0.9 Na, 0.1 K_2SO_4)-induced hot corrosion of the Ni-based superalloy M38G at 900°C in air. Electrochimica Acta 50: 5533-5538.